ELSEVIER

Biophysical Chemistry 109 (2004) 169–188

Biophysical Chemistry

www.elsevier.com/locate/bpc

Cloud-point temperatures of lysozyme in electrolyte solutions by thermooptical analysis technique

Eung Jo Park, Young Chan Bae*

Division of Chemical Engineering, Molecular Thermodynamics Laboratory, Hanyang University, Sungdonggu, Seoul 133-791, South Korea

Received 18 July 2003; received in revised form 5 November 2003; accepted 6 November 2003

Abstract

Liquid–liquid phase-separation data are obtained for aqueous solutions of lysozyme. Thermooptical analysis (TOA) technique overcomes many defects of the light scattering method, which is most commonly used for this purpose, and provides a simple, rapid and reliable experimental method to determine cloud-point temperatures (CPTs) of aqueous protein solution systems. The TOA apparatus described here needs very small amount of samples (0.02 ml), and CPT can easily be determined in a very short time. The CPTs are measured as a function of salt type and concentration at pH 4.0 and 7.0. Salts used include those from mono and divalent cations and anions, and the modified Perturbed-Hard-Sphere-Chain (PHSC) model that takes into account the shape of protein is used to interpret the effect of salts.

Keywords: Cloud-point temperature; Lysozyme; Phase transition; Specific ion effect; Thermooptical analysis

1. Introduction

Association of biomacromolecules is essential for the cellular structure and function; examples are provided by a protein nucleic-acid binding and protein–protein binding [1]. However, the protein association can also be detrimental to cellular function as, e.g. in the formation of cataracts and β-amyloid plaques [2,3]. Non-covalent forces including Coulombic, van der Waals and hydrophobic forces govern protein interactions. While these forces are understood on the level of small molecules, they remain obscure for complex macromolecules such as proteins.

Protein precipitation and crystallization are fundamental procedures to recover and characterize all proteins in application fields such as biotechnology and pharmaceutical industry. However, because protein interactions are governed by many factors, such as pH, surface hydrophobicity, surface-charge distribution, salt-type and salt concentration [4–6], the protein phase behavior is not well understood. Especially, lysozyme is well suited for such studies, since it is a robust and compact globular protein that is soluble over a broad range of conditions. It is available at high purity and has

*Corresponding author. Tel.: +82-222980529; fax: +82-222960568.

E-mail address: ycbae@hanyang.ac.kr (Y.C. Bae).

0301-4622/04/$ - see front matter © 2003 Elsevier B.V. All rights reserved.
doi:10.1016/j.bpc.2003.11.001

been studied extensively, making it suitable for the investigation of the protein-solution behavior. The well known method to investigate the protein-solution interactions is CPT measurements. CPTs also provide a guide to the net attractive interactions, which are related qualitatively to the crystallization temperatures, which is experimentally and theoretically used by many scientists [7–13]. There are also cases in which the protein crystal nucleation is researched [14–20].

This work discusses a simple and efficient thermooptical analysis technique for measuring liquid–liquid equilibria (LLE) of lysozyme in electrolyte solutions. About two decades ago, pulse-induced critical scattering (PICS) was developed to study the onset of phase separation in polymer systems. However, it is too expensive and difficult to operate [21–24]. PICS is designed to measure spinodal and cloud-point temperatures of polymer solutions. Our work uses a simple, yet precise method for measurement of liquid–liquid phase in protein solution systems. It is called thermooptical analysis (TOA) technique. We describe a particular TOA apparatus that yields data rapidly and requires only very small amount of samples.

We speculate on the specific effect of each of salt's cations and anions experimentally and theoretically, as its presence was indicated by Muschol and Rosenberger [25], rather than researching on the effect of salts as a whole [26–30]. There are cases in which effects of some ions are studied [31–33], however, we tried to cover all kinds of commonly used salt ions.

2. Experimental

2.1. Protein/salt solution preparation

Lysozyme, reagent-grade NaCl, $NaNO_3$, Na_2SO_4, NH_4Cl, $MgCl_2$, NH_4NO_3, $Mg(NO_3)_2$, $(NH_4)_2SO_4$, $MgSO_4$, Tris buffer and sodium azide were purchased from Aldrich. A 1 l stock solution of 20-mM Tris buffer was prepared. Lysozyme was dissolved in a small volume of the stock solution, and then sodium azide was added to the protein solution at a concentration of 2 mM to prevent bacterial growth. A salt is dissolved with desired concentration. The pH of the solution was adjusted with concentrated HCl or NaOH. The pH of each solution was checked after mixing.

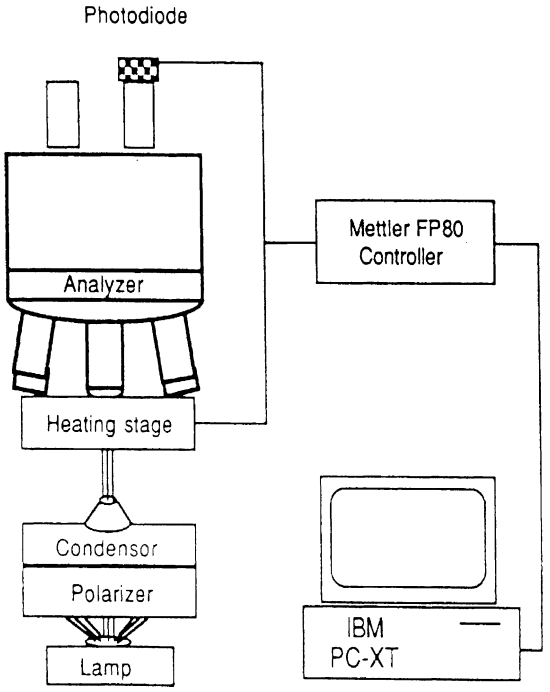

Fig. 1. Schematic of the apparatus for thermooptical analysis (TOA).

2.2. Sample preparation

We used a filling method similar to that described by Malcolm and Rowlinson [34]. The tube was collapsed and sealed when one end was heated by a flame while the content of the tube was maintained at subambient temperature by liquid nitrogen. An LPG/oxygen flame was used for sealing. Its temperature was high enough to seal a pyrex tube in <2 s. Using this method, we avoid the concentration change and the contamination of a sample while measuring CPTs.

2.3. Apparatus

Fig. 1 shows the experimental apparatus for TOA. The heating-cooling stage is designed for observation of the thermal behavior of a sample

under the microscope. Luminosity in the observation field is measured by a photodiode and recorded on the PC. The temperature program for the given run is entered into the microprocessor. This program consists of a starting temperature, a heating and cooling rate, and an end temperature. Results shown on the microprocessor display are connected to the PC for data storage. The temperature of the system can be varied from −60 to +300 °C with scan rates as low as 0.1 °C/min for both heating and cooling. For experiments below room temperature, the stage coolant inlet is connected to a cooling coil immersed in liquid nitrogen. The coolant air passes through the inlet to the fan and is blown sideways between the external and internal housing of the stage. In the stage, sample temperature is controlled by both the upper and lower plates, assuming symmetric heat distribution through the sample. In this way, equilibrium time can be shortened since the sample cell is directly in contact with the heating unit and the amount of sample is only 0.02 ml. Temperature, measured by a platinum resistance thermometer, is stored on a PC. The photodiode quantitatively measures the intensity of the transmitted light as a function of temperature; these data are used to determine the cloud points of protein solutions.

2.4. Advantages of our TOA technique

In the apparatus described here, equilibrium is attained rapidly first, because the sample is very small (0.02 ml) and, second, because the sample is in direct contact with the heater or cooler. In conventional CPT measurement apparatus, equilibrium is not attained as rapidly because the sample is ~1 order of magnitude larger and because heat transfer must go through a bath containing the sample.

2.5. Cloud-point temperature measurements

A sealed sample tube was placed and centered in the microscope heating–cooling stage and the photodiode with the light source of the microscope was calibrated for the following measurement. To find the range of cloud points of the sample, a high scan rate of heating or cooling (1 °C/min) was used. In this way, the approximate cloud point of the sample was found. The sample was then repeatedly heated or cooled over a temperature range near the cloud point with a low scan rate (0.1 °C/min) while the intensity of light was monitored. The photodiode permitted quantitative determination and recording of the light intensity of the field of view as a function of temperature. Each measurement was repeated at least three times to assure reproducibility. Fig. 2 shows a typical result for cloud-point temperature determination by cooling a sample, which is the CPT of aqueous lysozyme solution with 1.8 M $(NH_4)_2SO_4$ at pH 4.0. The first phase separation observed (corresponding to the point of abrupt transition of luminosity) was then recorded as the cloud-point temperature of the sample at the given condition.

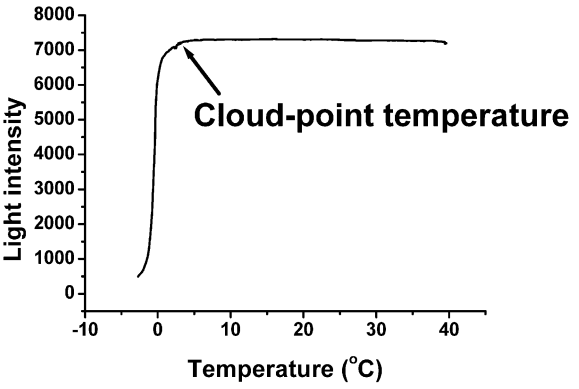

Fig. 2. A typical result for cloud-point temperature determination by cooling a sample. (1.8 M $(NH_4)_2SO_4$ at pH 4.0).

3. Theoretical Consideration

To provide a means of predicting the CPT, we employ a square-well potential of mean force $W(r)$ to describe the interactions of two lysozyme molecules:

$$W(r)=\begin{cases}\infty & r<\sigma\\ -\varepsilon & \sigma\le r\le\sigma+\delta\\ 0 & \sigma+\delta<r\end{cases} \quad (1)$$

where r is the center-to-center distance between

two protein molecules, σ is the protein diameter, ε is the depth and δ is the width of the square well. The width of the square well is assumed to be 20% of the protein diameter as suggested by Frenkel [35,36]. We set $\sigma = 34.4$ Å, the hard sphere diameter of a lysozyme molecule determined from X-ray crystallography. Hence, $\sigma = (0.2)(34.4\ \text{Å}) = 6.9$ A.

To describe liquid–liquid equilibria, we use the Random Phase Approximation(RPA) to generate expressions for the pressure and chemical potential [37]. We employ the generalized van der Waals partition function, which is proposed by Chang and Bae [38]. The partition function Q depends on temperature T, system volume V and number of protein molecules N. The generalized van der Waals partition function [39] for a hard sphere fluid is given:

$$Q(T,V,N) = \frac{1}{N!}\left(\frac{V}{\Lambda^3}\right)^N \left(\frac{V_f}{V}\right)^N \left[\exp\left(\frac{-E_0}{2k_B T}\right)\right]^N (q_{r,v})^N \tag{2}$$

where Λ is the de Broglie wavelength and the free volume V_f is the volume available to the center of mass of a molecule. E_0 is the intermolecular potential energy of one molecule due to the attractive forces from all other molecules. The contribution per molecule from rotational and vibrational degree of freedom, $q_{r,v}$, is a unit $(=1)$ for a perfect sphere molecule. For large molecules, $q_{r,v}$ depends significantly on density, when the molecules deviate from the spherical shape. Donohue [40] proposed the expression of $q_{r,v}$:

$$q_{r,v}(V,T) = \left[\frac{V_f}{V}\exp\left(-\frac{E_0}{2kT}\right)\right]^{c-1} \tag{3}$$

where $3c$ is the total number of effective external degree of freedom per molecule. It is well known that shapes of most proteins are not perfectly spherical. In this work, we replace c by τ_{ps} to take into account the effect of protein shape in the partition function, Q. It is assumed that τ_{ps} affects to the potential of mean force and $q_{r,v}$, simultaneously Eq. (2) is replaced by

$$Q(T,V,N) = \frac{1}{N!}\left(\frac{V}{\Lambda^3}\right)^N \left(\frac{V_f}{V}\right)^N \left[\exp\left(\frac{-\bar{E}_0}{2k_B T}\right)\right]^N \left(\frac{V_f}{V}\exp\left(\frac{-\bar{E}_0}{2k_B T}\right)\right)^{N(\tau_{ps}-1)}$$

$$= \frac{1}{N!}\left(\frac{V}{\Lambda^3}\right)^N \left(\frac{V_f}{V}\exp\left(\frac{-\bar{E}_0}{2k_B T}\right)\right)^{N\cdot\tau_{ps}} \tag{4}$$

where $\bar{E}_0 = \tau_{ps} E_0$, which is the intermolecular potential energy of a non-spherical protein due to the attractive forces from all other proteins. The fact is found in literatures [41] that the interacting types between non-spherical molecules affect the intermolecular potential energies. Therefore, τ_{ps} reflects the rotational and vibrational contributions per a protein molecule that are affected by the presence of non-spherical proteins. In this work, we assume that the difference between $\bar{E}_0$ and E_0 originated from non-sphericality is mainly due to the additional volume of a non-spherical molecule.

$$\upsilon_{non} = \upsilon_{sph} + \delta\upsilon_{add} = \upsilon_{sph}\left(1 + \frac{\delta\upsilon_{add}}{\upsilon_{sph}}\right) = \upsilon_{sph}\cdot\tau_{ps} \tag{5}$$

where υ represents the volume of a protein molecule and subscript 'non', 'sph' and 'add' stand for non-spherical, spherical and additional, respectively. τ_{ps} is defined by the geometric mean of the ratio of σ_{pi} to σ_p:

$$\tau_{ps} = \left(1 + \frac{\delta\upsilon_{add}}{\upsilon_{sph}}\right)$$

$$\approx \left(\prod_{j=1}^{n} \sigma_{pi}/\sigma_p^n\right)^{1/n} \approx \left(\frac{\sigma_{px}\sigma_{py}\sigma_{pz}}{\sigma_p^3}\right)^{1/3} \tag{6}$$

where $n = 3$ due to the experimental accessibility [42,43] and simplicity. x, y and z are 3-directional

axes and σ_{pi} is *i*-directional crytstallographic unhydrated diameter. The larger value of τ_{ps} means that the each directional protein diameter deviates more from the unhydrated hard sphere diameter. When $\tau_{ps}=1$, i.e. a perfect hard sphere, Q reduces to the classical van der Waals-type perturbed-hard-sphere theory.

The equation of state is related

$$P=k_BT\left(\frac{\partial \ln\ Q}{\partial V}\right)_{T,N} \tag{7}$$

Substituting Eq. (4) into Eq. (7) with $V_f=V\exp\left[\frac{\eta(3\eta-4)}{(1-\eta)^2}\right]$, Carnahan–Starling expression, yields:

$$\left(\frac{P}{\rho k_BT}\right)=1+\frac{\tau_{ps}(4\eta-2\eta^2)}{(1-\eta)^3}+\frac{\tau_{ps}^2\rho U}{2k_BT} \tag{8}$$

where $\rho\left(=\frac{N}{V}\right)$ is the number density of protein molecules. In Eq. (8), τ_{ps}, which results from the third term in Eq. (4), corrects both the underestimated hard sphere contribution and attractive perturbation. Especially, the packing fraction, η, is defined as follows:

$$\eta=\eta_{sph}+\delta\eta_{add}=\frac{\pi\rho\sigma_p^3}{6}\left(1+\frac{\delta\eta_{add}}{\eta_{sph}}\right)=\eta_{sph}\cdot\tau_{ps} \tag{9}$$

and U is the perturbation energy per unit density,

$$U=-\frac{E_0}{\rho}=4\pi\int W_{pp}(r)r^2\mathrm{d}r \tag{10}$$

where $W_{pp}(r)$ is the sum of the potentials-of-mean-force.

The general equation for calculating the Helmholtz energy from a pressure-explicit equation of state [44] is

$$\frac{A}{Nk_BT}=\frac{A^0}{Nk_BT}+\int_0^\rho\left(P/\rho k_BT-1\right)\frac{\mathrm{d}\rho}{\rho}$$

$$=\frac{A^0}{Nk_BT}+\frac{\tau_{ps}(4\eta-3\eta^2)}{(1-\eta)^2}+\frac{\rho\tau_{ps}^2U}{2k_BT} \tag{11}$$

where $A^0(T)$ is the Helmholtz energy at standard state.

The chemical potential is

$$\mu=\left(\frac{\partial A}{\partial N}\right)_{T,V} \tag{12}$$

and substituting Eq. (11) into Eq. (12) yields

$$\frac{\Delta\mu}{k_BT}=\frac{\mu}{k_BT}-\frac{\mu^0}{k_BT}=\frac{\tau_{ps}(8\eta-9\eta^2+3\eta^3)}{(1-\eta)^3}+\ln\ \rho+\frac{\tau_{ps}^2\rho U}{k_BT} \tag{13}$$

At equilibrium, protein concentrations in the supernatant and dense-fluid phases are calculated from Eqs. (14) and (15) based on the classical equilibrium conditions:

$$\Delta\mu^s=\Delta\mu^d \tag{14}$$

$$P^s=P^d \tag{15}$$

where superscripts '*s*' and '*d*' denote the supernatant and dense phases, respectively.

Because at the onset of clouding, the volume of the dense phase that forms is negligibly small compared to the total volume, the protein concentration in the supernatant phase is equal to the initial protein concentration. There are two unknowns in Eqs. (14) and (15), ε and the protein packing fraction in the dense phase, η^β. Input parameters are the known initial protein packing fraction, η^α and the measured CPT.

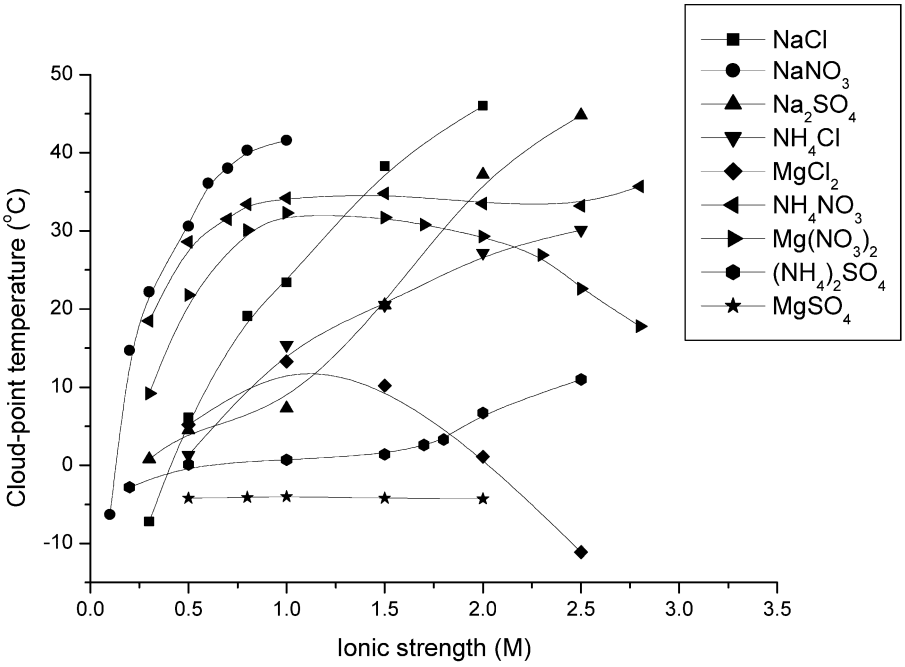

Fig. 3. Cloud-point temperatures at pH 4.0.

Toward interpreting the significance of the inter-protein energy parameter ε, we employ the idea proposed by Grisby et al. [45]. For comparison of salts, NaCl was chosen as a 'reference salt' because Na^+ is marginally kosmotropic and Cl^- is marginally chaotropic. The difference between the entropy of pure water and the entropy of water near Na^+ or Cl^- is nearly zero [46,47]. Although Cl^- has been shown to bind to lysozyme [48–50], any subsequent solution restructuring at the ion-binding site can be considered to be minimal compared to highly kosmotropic or chaotropic ions. Using CPT data for lysozyme solution containing NaCl, ε was calculated as a function of salt concentration at pH 4.0 and 7.0.

At a fixed ionic strength, deviations of the CPT for a salt relative to that for NaCl were attributed to specific ion interactions with lysozyme. For all salts except NaCl, a change in the square-well potential was introduced to account for these specific ion effects and is given by:

$$W(r) = -[\varepsilon_{\mathrm{NaCl}}(I) + \varepsilon_{\mathrm{sp}}(I)] \quad (16)$$

where I is the ionic strength. To calculate $\varepsilon_{\mathrm{sp}}$, we use as input the calculated $\varepsilon_{\mathrm{NaCl}}(I)$, the known initial protein packing fraction η^{α} and the measured CPT of the salt.

4. Results and discussion

Figs. 3 and 4 show CPTs at pH 4.0 and 7.0, respectively. All the data are listed in Tables 1 and 2. The CPT results depend strongly on the specific nature of the ions. Kosmotropic ions bind adjacent water molecules more strongly than water binds itself. When a kosmotropic ion is introduced into water, the entropy of the system decreases due to increased water structuring around the ion. In contrast, chaotropes bind adjacent water molecules less strongly than water binds itself. When a chaotrope is introduced into water, the entropy of the system increases because the water structuring around the ion is less than that of the salt-free water. This classification is related to the size and charge of the ion. Ions with high charge density such as Mg^{2+}, Ca^{2+} and SO_4^{2-} are highly kosmotropic. Ions with low charge density such as K^+, NH_4^+ and NO_3^- are chaotropic, especially,

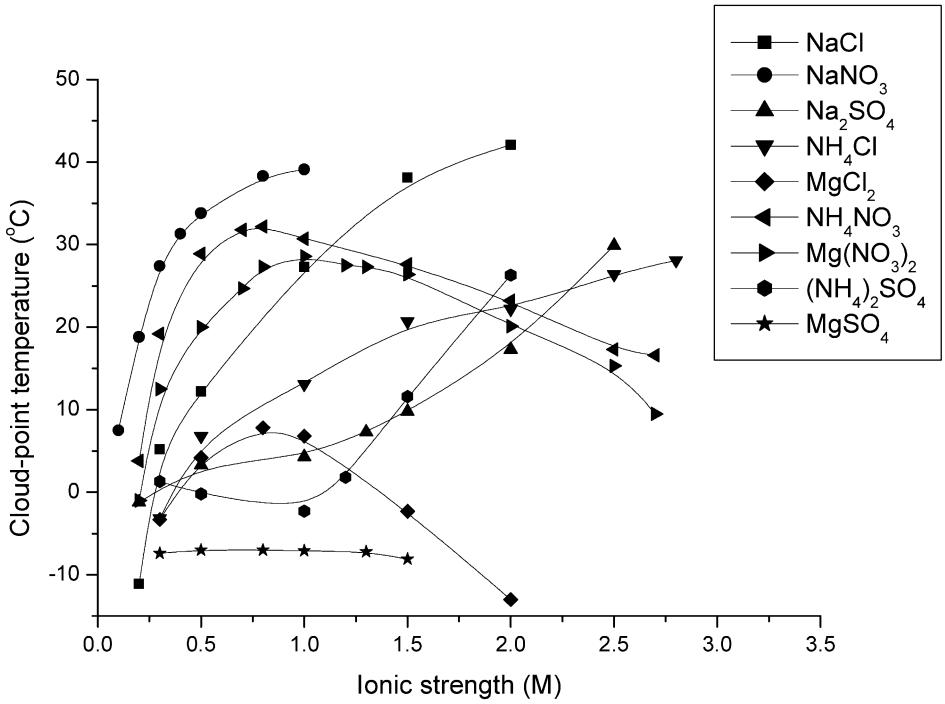

Fig. 4. Cloud-point temperatures at pH 7.0.

NO_3^- is strongly chaotropic. Na^+ is weakly kosmotropic and Cl^- is weakly chaotropic [51]. We discuss the CPT results in terms of the chaotropic or kosmotropic nature of anions and cations.

The effect of cation at pH 4.0 and 7.0 are shown in Figs. 5 and 6, respectively. For the monovalent cations, the CPT increases with the salt concentration. For divalent cations, as the salt concentration rises, the maximum CPT is observed and attributed to the ion binding for the protein surface and subsequent water structuring. The trends are similar at both pHs. For different salts, as the ionic strength decreases, the difference in CPT declines, indicating that the specific nature of the ion is less important at an ionic strength below 0.3 M. CPT measurements were not be observed at low salt concentration ranges because the solution formed ice crystals before a liquid–liquid phase separation was observed. The difference in CPT becomes dramatic for different salt types above the ionic strength of 0.3 M. CPT increases less sharply with ionic strength for NH_4Cl than that for NaCl. For the divalent salt $MgCl_2$, a maximum CPT is observed at the ionic strength of 0.8 M, pH 7.0 and at 1.0 M, pH 4.0. It is due to the binding of the highly kosmotropic ion Mg^{2+} to the protein. Ion binding to the protein surface and subsequent structuring of water around the ion produces a repulsive barrier, which is the hydration force. Hydration forces may be observed from surface-force measurements. At very short separation distances less than 2 nm, charged bilayers adsorbed on mica surfaces are repulsive. It is due to steric hydration interactions between the hydrophilic headgroups that characterize the surface [52]. Pashley has shown that the interaction between bare mica surfaces in concentrated electrolyte solutions gives rise to a repulsive hydration force that follows from the binding of hydrated cations to the negatively charged surfaces [53–57]. The magnitude of this force is related to the energy needed to dehydrate the bound cations, which retain some of their water of hydration upon binding. The strength and range of hydration forces increase

Table 1
Cloud-point temperatures at pH 4.0

NaCl	
Concentration (M)	Cloud-point temperature (°C)
$Mg(NO_3)_2$	
0.3	−7.2
0.5	6.1
0.8	19.1
1	23.4
1.5	38.3
2	46
$NaNO_3$	
0.1	−6.3
0.2	14.7
0.3	22.2
0.5	30.6
0.6	36.1
0.7	38
0.8	40.3
1	41.6
Na_2SO_4	
0.3	0.8
0.5	4.5
1	7.3
1.5	20.5
2	37.2
2.5	44.8
NH_4Cl	
0.5	1.3
1	15.4
1.5	20.5
2	27.2
2.5	30.1
$MgCl_2$	
0.5	5.2
1	13.3
1.5	10.2
2	1.1
2.5	−11.1
NH_4NO_3	
0.3	18.5
0.5	28.6
0.7	31.5
0.8	33.4
1	34.2
1.5	34.8
2	33.5
2.5	33.2
2.8	35.7
$Mg(NO_3)_2$	
0.3	9.2
0.5	21.8
0.8	30.1
1	32.3
1.5	31.7
1.7	30.8
2	29.3
2.3	26.9
2.5	22.6
2.8	17.8
$(NH_4)_2SO_4$	
0.2	−2.8
0.5	0.1
1	0.7
1.5	1.4
1.7	2.6
1.8	3.3
2	6.7
2.5	11
$MgSO_4$	
0.5	4.2
0.8	4.1
1	4
1.5	4.2
2	4.3

with the hydration number of the cation. When a kosmotropic ion binds to an oppositely charged residue on the protein surface, the extent of water structuring at the protein surface increases. Chaotropes do not interact strongly with oppositely charged residues on the protein surface due to their low charge density, but tend to disrupt the structure of water in the bulk solution. For two protein molecules to approach each other to form a second, more-dense phase, the water structure surrounding the protein surface must be broken. As the concentration of the divalent cation increases, the extent of ion binding and subsequent water structuring at the surface increases. The repulsive hydration force grows with the salt concentration. The second more-dense liquid phase becomes energetically unfavorable at higher salt concentrations due to the rise in the repulsive hydration force. Therefore, the CPT falls at higher salt concentrations. CPT measurements could not be taken at higher salt concentrations for $NaNO_3$ due to the appearance of irreversible aggregates at

Table 2
Cloud-point temperatures at pH 7.0

NaCl	
Concentration (M)	Cloud-point temperature (°C)
0.2	−11.1
0.3	5.2
0.5	12.2
1	27.3
1.5	38.1
2	42.1
$NaNO_3$	
0.1	7.5
0.2	18.8
0.3	27.4
0.4	31.3
0.5	33.8
0.8	38.3
1	39.1
Na_2SO_4	
0.2	−1.2
0.5	3.3
1	4.3
1.3	7.3
1.5	9.8
2	17.3
2.5	29.9
NH_4Cl	
0.3	−3.2
0.5	6.8
1	13.1
1.5	20.7
2	22.2
2.5	26.4
2.8	28.1
$MgCl_2$	
0.3	−3.3
0.5	4.2
0.8	7.8
1	6.8
1.5	−2.3
2	−13
NH_4NO_3	
0.2	3.8
0.3	19.2
0.5	28.9
0.7	31.8
0.8	32.2
1	30.7
1.5	27.6
2	23.2
2.5	17.3
2.7	16.6
$Mg(NO_3)_2$	
0.2	−1
0.3	12.5
0.5	20
0.7	24.7
0.8	27.3
1	28.6
1.2	27.5
1.3	27.3
1.5	26.4
2	20.1
2.5	15.3
2.7	9.5
$(NH_4)_2SO_4$	
0.3	1.3
0.5	−0.2
1	−2.3
1.2	1.8
1.5	11.6
2	26.3
$MgSO_4$	
0.3	7.4
0.5	7
0.8	7
1	7.1
1.3	7.2
1.5	8.1

temperatures above 45 °C, possibly because of the thermal protein denaturation. For the sulfate series, CPT trends are significantly different from those for chloride and nitrate salts. It is known that lyotropic series for lysozyme is reversely relative to most proteins [58]. The sulfate ion, a good salting-in ion for lysozyme, has been shown to be preferentially excluded at the lysozyme surface [59,60]. When compared to chloride and nitrate salts, the CPT increases at much slower rate as the salt concentration rises. Above the ionic strength of 1.0 M, CPT begins to rise dramatically for Na_2SO_4 and $(NH_4)_2SO_4$. This rise is due to a competition for water to hydrate the protein surface or the sulfate ion. The sulfate ion is highly kosmotropic and therefore, interacts strongly with water molecules. At low salt concentrations, the solution contains a sufficient number of water molecules to hydrate both the protein surface and

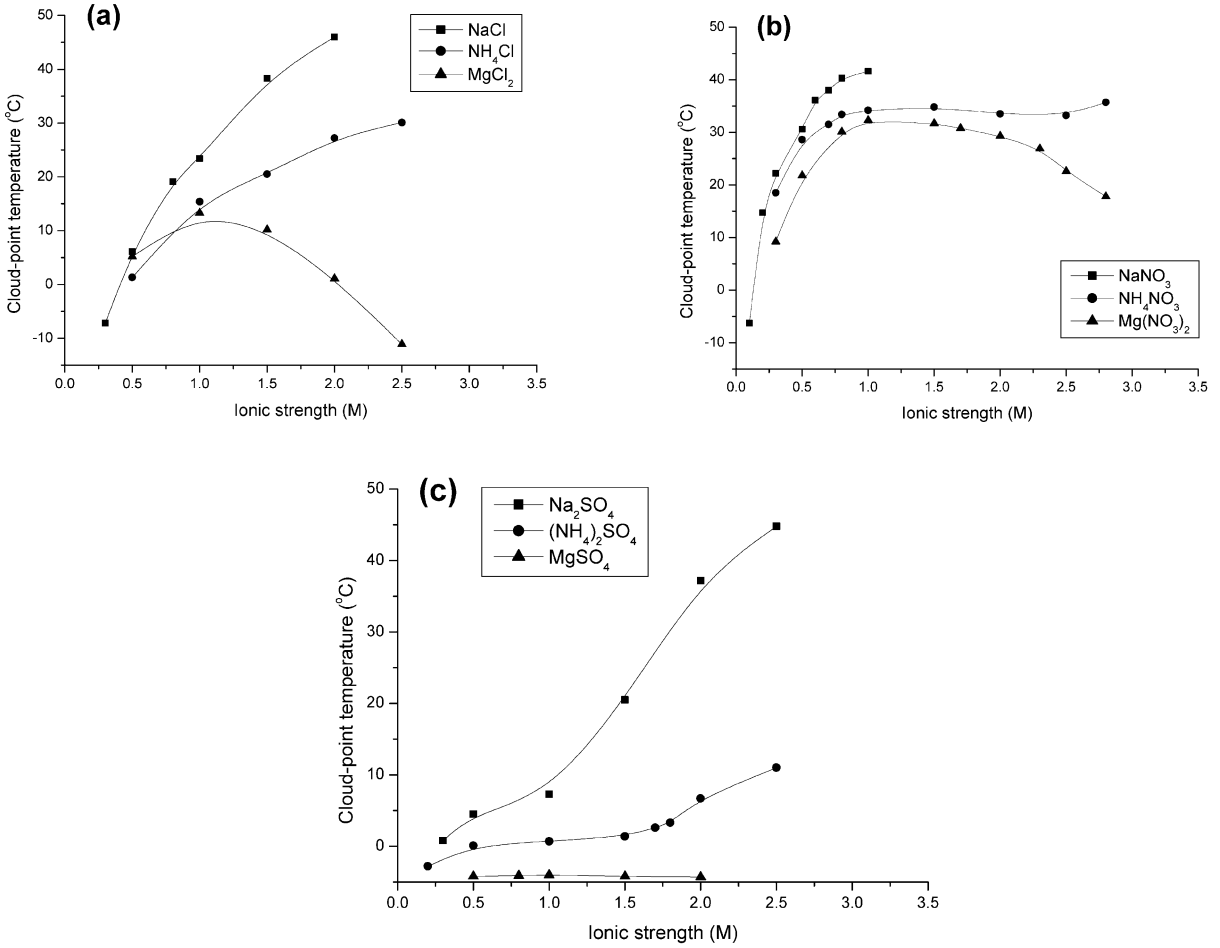

Fig. 5. Effect of cation at pH 4.0 for (a) Cl^- (b) NO_3^- (c) SO_4^{2-}.

the sulfate ions. At higher salt concentrations, more water molecules are needed to hydrate the increasing number of sulfate ions. A formation of the second more dense protein phase provides more free water molecules to hydrate the sulfate ions because of the lower number of water molecules needed to hydrate protein molecules in the dense phase. The maximum CPT is observed for $MgSO_4$, but the CPT does not change significantly over the entire salt concentration range. The effects of the magnesium and sulfate ions appear to cancel each other at higher salt concentrations. Magnesium ion preferentially interacts at the protein surface leading to a repulsive hydration force while the sulfate ion dehydrates the protein surface leading to an attractive force.

Figs. 7 and 8 represent the effect of anion at pH 4.0 and 7.0, respectively. For anions at fixed salt concentration, the CPT decreases with the anion kosmotropic character. In all plots, as the anion becomes more kosmotropic, the CPT decreases with a specific salt concentration. This specificity follows from the extent of water structuring in the system. Sulfate is highly kosmotropic, chloride marginally chaotropic and nitrate very chaotropic. There is a greater solution structure for sulfate salts compared to nitrate salts. The greater the solution structure, the greater the repulsive

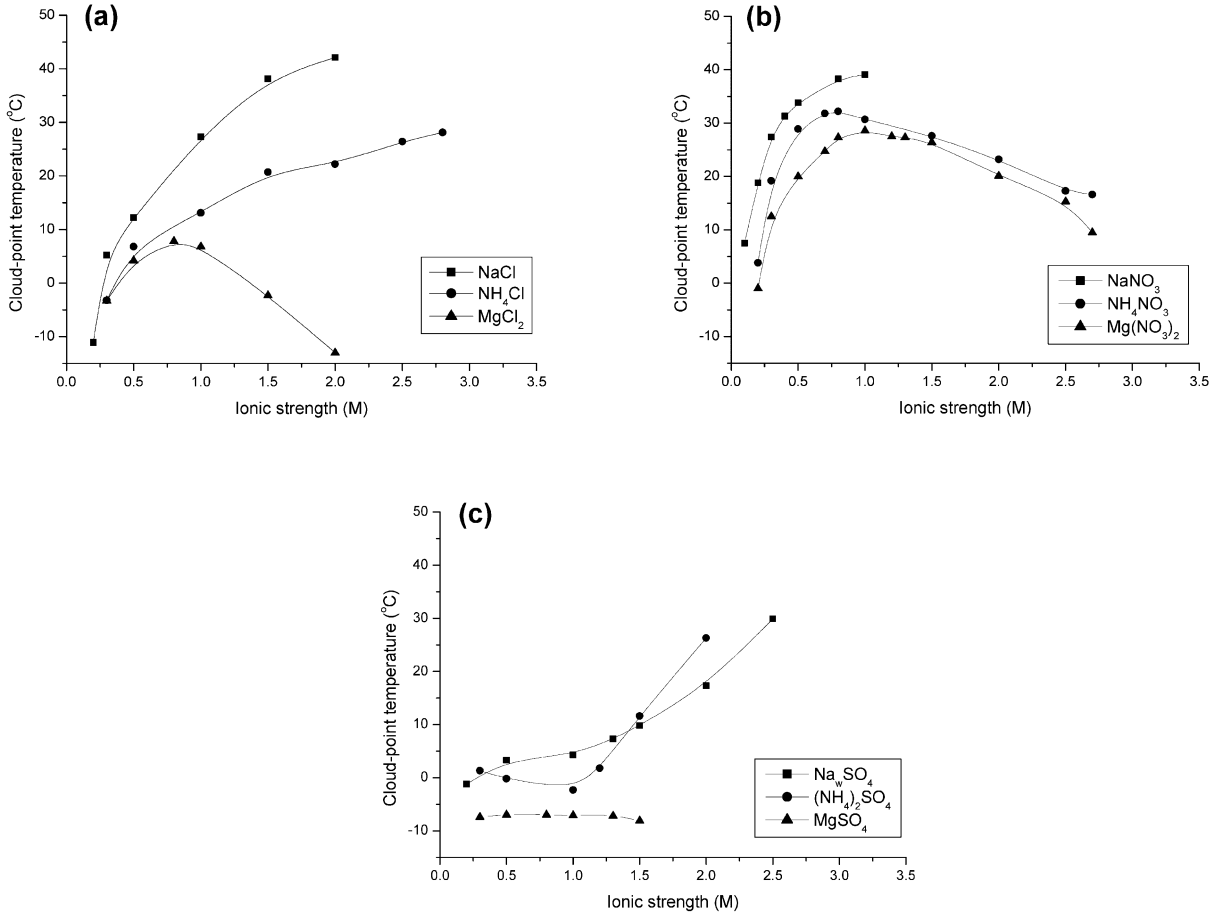

Fig. 6. Effect of cation at pH 7.0 for (a) Cl^- (b) NO_3^- (c) SO_4^{2-}.

hydration force and, hence this leads to a lower CPT.

The effect of pH is shown in Fig. 9. Comparison of CPTs for pH 4.0 and 7.0 revealed two trends. At low ionic strength for a given salt, differences in CPT can be explained in terms of repulsive electrostatic interactions between protein molecules, while at higher ionic strength, differences can be attributed to hydration forces. In addition, the nitrate salts follow the same trends as that of the chloride salts. As the concentration of salt rises, the difference between the CPT at both two pHs decreases and disappears at the ionic strength above 1.3 M. This decrease and disappearance follow from the salt screening of the charge-charge repulsion between protein molecules. The net charge of lysozyme is +11 at pH 4.0 and +8 at pH 7.0, respectively. At a fixed salt concentration below 1.3 M, the net attractive interactions measured by the CPT at pH 4.0 are less than those at pH 7.0 due to greater charge-charge repulsion at this pH. As the concentration of salt increases, the repulsive charge-charge interaction between proteins vanishes because it is screened by the salt ions. This trend can be seen in all CPT data at low salt concentration ranges. The concentration where the charge-charge screening is complete depends on the nature of the ions. Fig. 5e compares the effect of pH on CPT for $MgCl_2$. Above the salt concentration where the charge screening

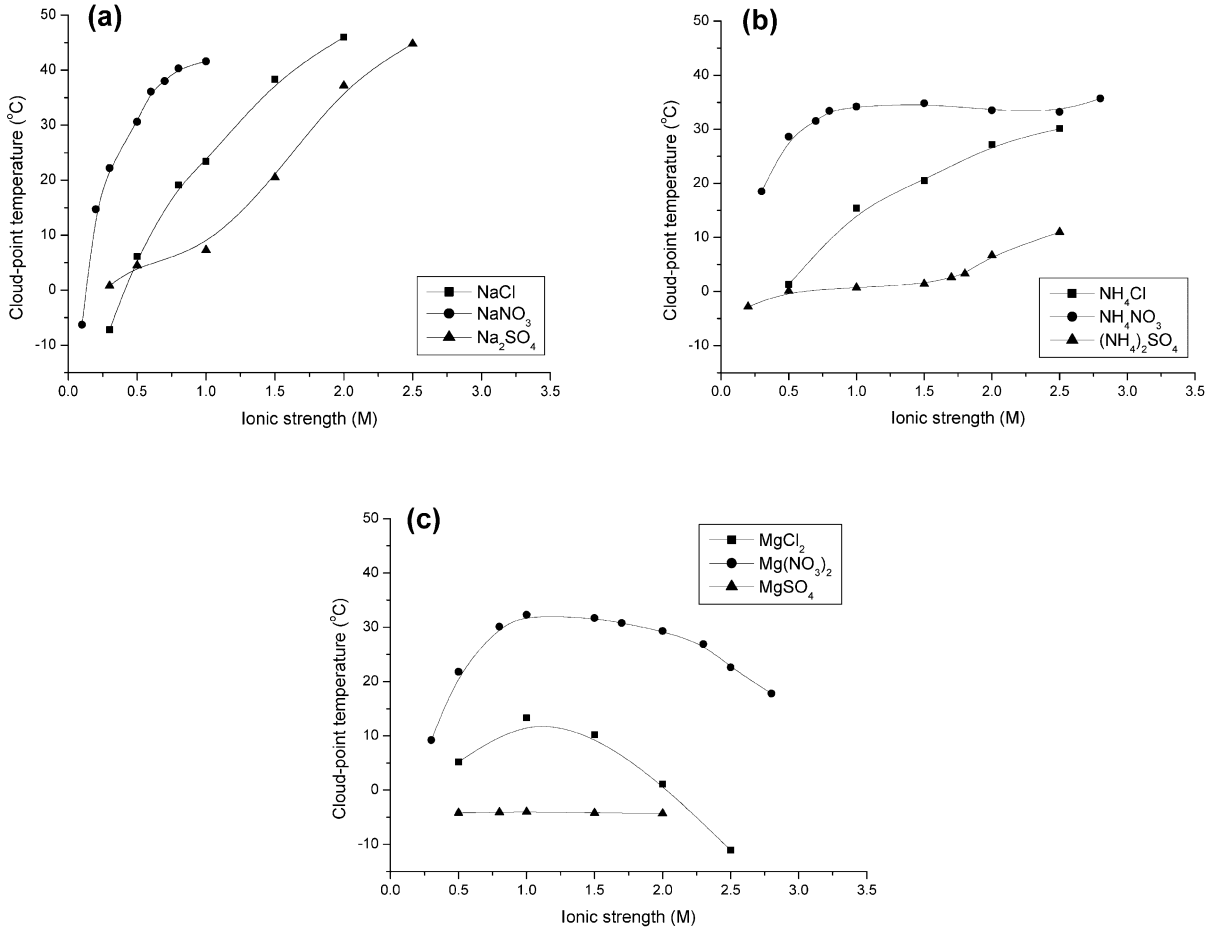

Fig. 7. Effect of anion at pH 4.0 for (a) Na^+ (b) NH_4^+ (c) Mg^{2+}.

occurs, CPT data begin to diverge. The difference between CPTs at pH 4.0 and 7.0 increases with the salt concentration. The CPT at pH 4.0 is always greater than that at pH 7.0. This difference follows from Mg^{2+} binding to the protein surface. Magnesium is a kosmotropic ion that has been shown to bind to the surface of lysozyme [61]. The number of ions that can bind to that surface depends on the protein charge. Because the net positive charge on the lysozyme molecule is less at pH 7.0, cations can bind to the surface more at pH 7.0 than at pH 4.0. Binding of kosmotropes to the surface of a protein produces more water structuring at the protein surface, leading to a hydration barrier to the protein aggregation. With the rising salt concentration, the extent of this hydration barrier increases, as indicated by CPT data. Although ammonium is not a kosmotropic ion, the CPT trends suggest that this ion is binding to the protein surface. The effect of pH on the CPT for sulfate salts differs from the trends seen in the chloride and nitrate salts. Significant differences in the CPT appear above 1 M due to the greater competition for binding water to the protein surface and to the sulfate ion.

The depth of the square well was calculated for the reference salt NaCl as a function of ionic strength for pH 4.0 and 7.0 at the CPT. Table 3

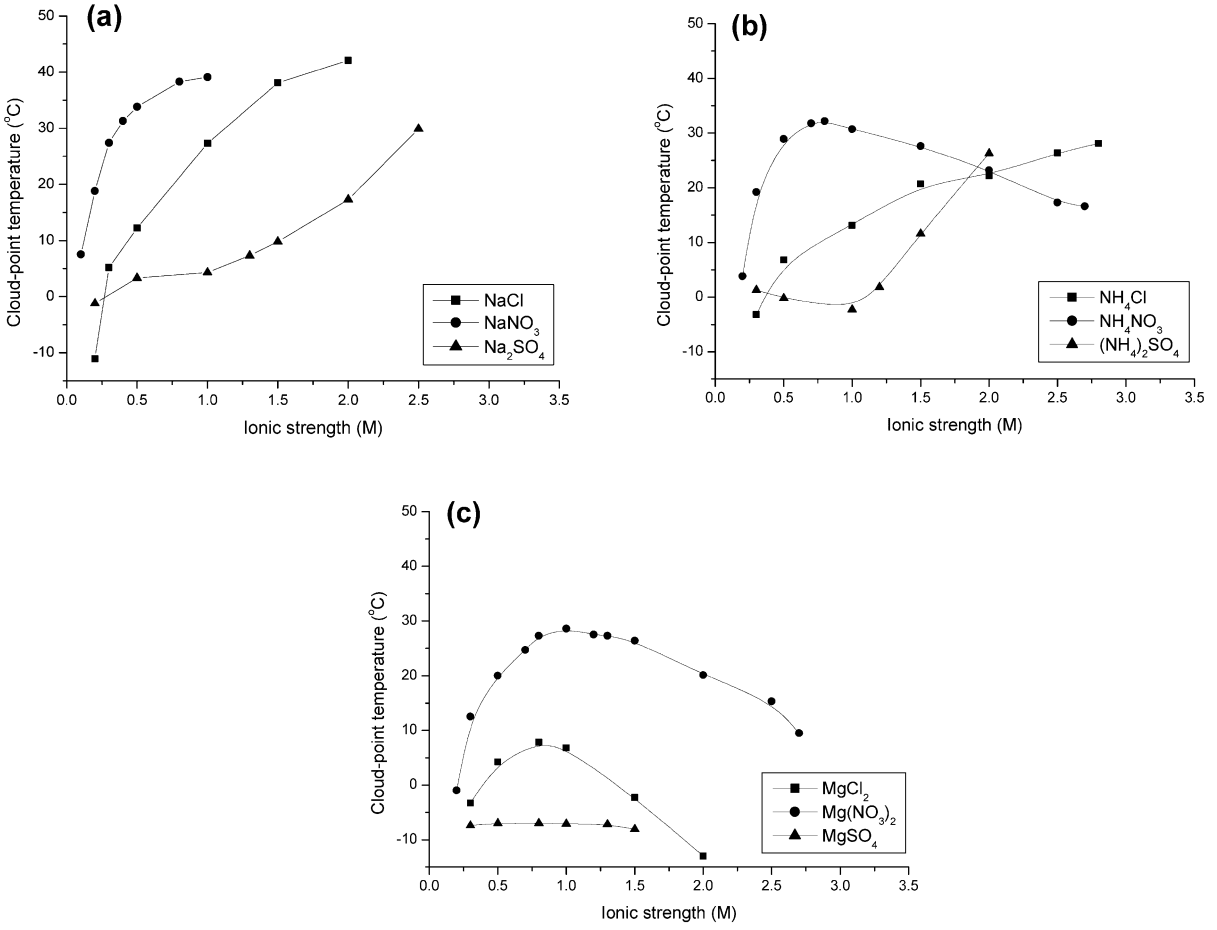

Fig. 8. Effect of anion at pH 7.0 for (a) Na^+ (b) NH_4^+ (c) Mg^{2+}.

shows calculated values of $\frac{\varepsilon}{kT}$ as a function of ionic strength for each salt.

Deviations from the reference in CPTs are due to the specific ion effect, including hydration forces and water structuring of the solution. To calculate the corresponding $\varepsilon_{sp}(I)$, equations in Table 3 were used in conjunction with CPT data for the other salts in Eq. (16). When needed, values for ε_{NaCl} were extrapolated beyond those obtained from measured CPTs for NaCl. Table 3 gives equations for $\frac{\varepsilon}{kT}$ at pH 4.0 and 7.0 at $T=$ 298.15 K.

For salts containing either Na^+ or Cl^-, the $\frac{\varepsilon}{kT}$ results in Table 3 reflect effects due to the appropriate counterion. For example, the $\frac{\varepsilon}{kT}$ values for $MgCl_2$ are attributed to the Mg^{2+} ion only. Combinations of $\frac{\varepsilon}{kT}$ for ions other than Na^+ or Cl^- can be used to calculate the CPT. This model is based on a fixed protein concentration of 87 g/l. Further CPT data are needed to assess whether $\frac{\varepsilon}{kT}$ is dependent on the protein concentration.

Combinations of $\frac{\varepsilon}{kT}$ for all ions were performed

and compared to $\frac{\varepsilon}{kT}$ values obtained through experimental and subsequent calculations. Fig. 10 shows results for combinations of (a) NH_4NO_3 at pH 4.0 (b) NH_4NO_3 at pH 7.0 (c) $Mg(NO_3)_2$ at pH 4.0 (d) $Mg(NO_3)_2$ at pH 7.0 (e) $(NH_4)_2SO_4$ at pH 4.0 (f) $(NH_4)_2SO_4$ at pH 7.0 (g) $MgSO_4$ at pH 4.0 (h) $MgSO_4$ at pH 7.0. The average of $\frac{\varepsilon}{kT}$ for all the salts showed good agreement with

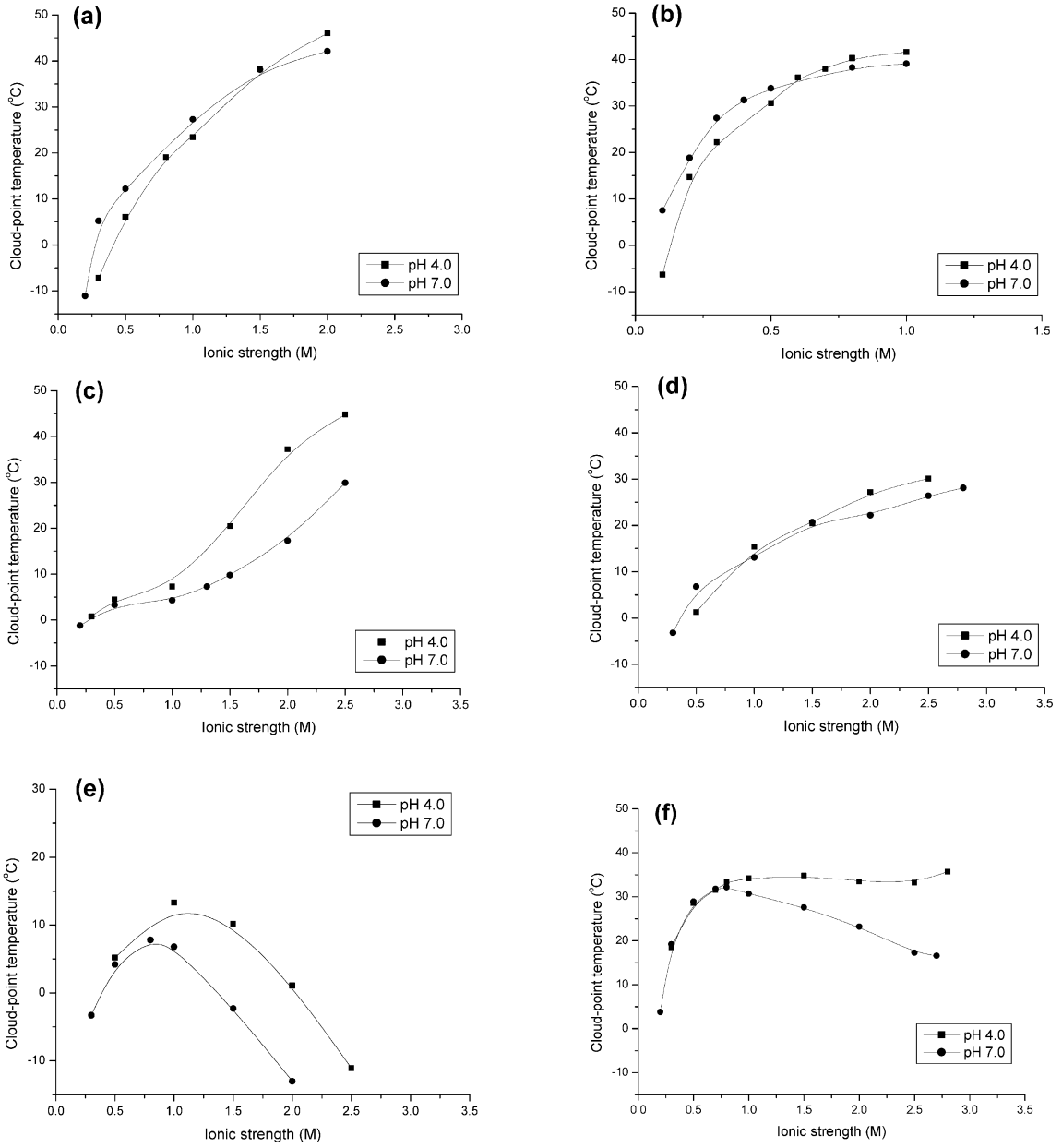

Fig. 9. Effect of pH for (a) NaCl (b) $NaNO_3$ (c) Na_2SO_4 (d) NH_4Cl (e) $MgCl_2$ (f) NH_4NO_3 (g) $Mg(NO_3)_2$ (h) $(NH_4)_2SO_4$ (i) $MgSO_4$.

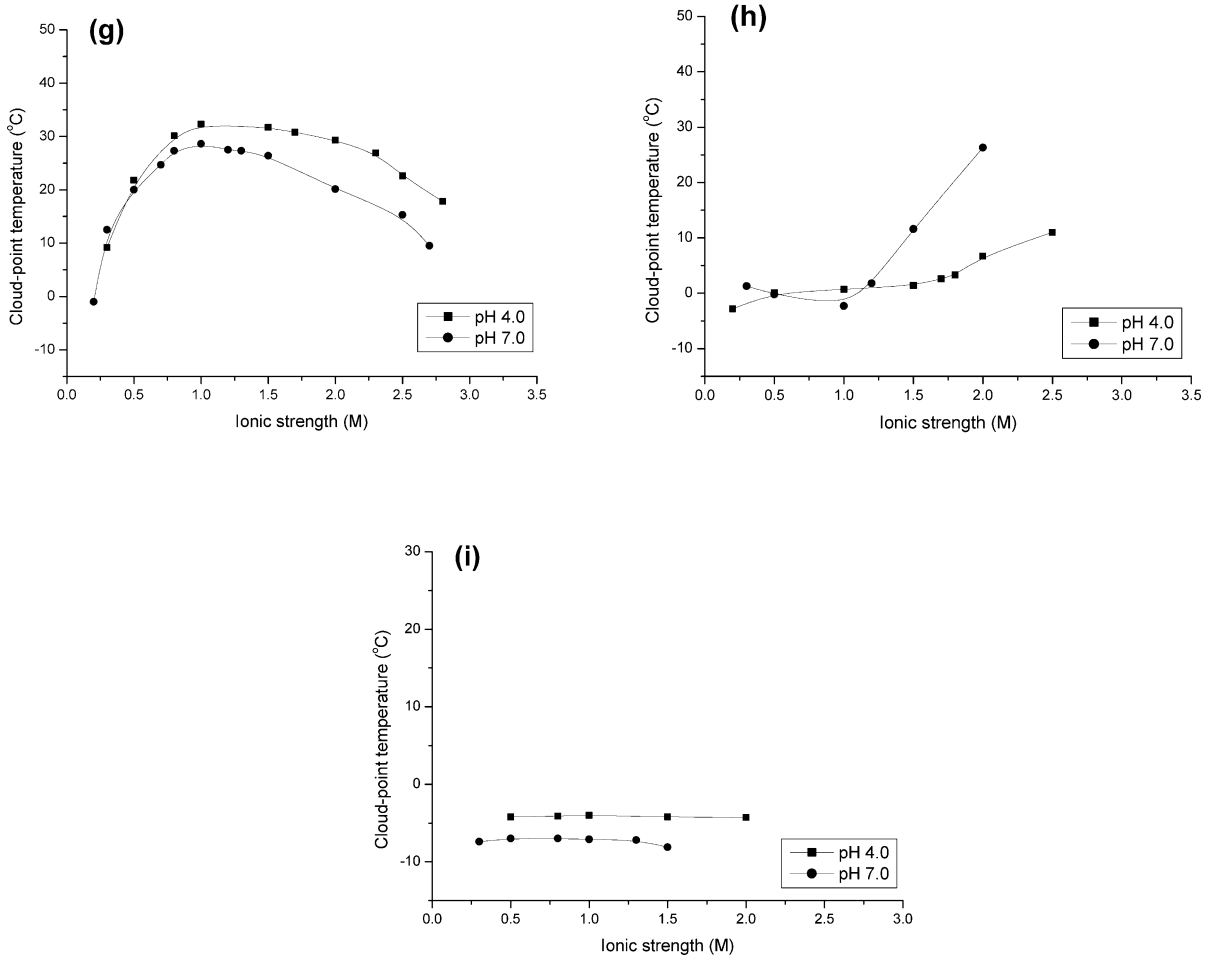

Fig. 9 (Continued).

experimentally measured CPT data for all ions, except $(NH_4)_2SO_4$, which overestimates the $\frac{\varepsilon}{kT}$ value. $\frac{\varepsilon}{kT}$ for NH_4NO_3 was predicted by the addition of $\frac{\varepsilon}{kT}$ for NH_4Cl and $NaNO_3$. Since NaCl is the reference salt, the contribution to $\frac{\varepsilon}{kT}$ by NH_4Cl is solely due to NH_4^+ since the contribution by Cl^- is zero. Similarly, the contribution to $\frac{\varepsilon}{kT}$ by $NaNO_3$ is solely due to NO_3^- since the contribution by Na^+ is zero. For another example, $\frac{\varepsilon}{kT}$ for Mg_2NO_3 was computed by adding equations from Table 3 for $MgCl_2$ and $NaNO_3$ and subsequently taking the average of the result. The reason why the average gives good results is due to the nature of the ions. Mg^{2+} and Ca^{2+} are highly kosmotropic and increase the extent of solution structure while the highly chaotropic ion NO_3^- breaks up the solution structure. The competing processes of increasing and decreasing the extent of water structure lead to an average effect.

Table 3
Relationship between the depth of the square well, ε, and ionic strength I M. ε was made dimensionless through division by kT where T was chosen to be 298.15 K

Salt	$\frac{\varepsilon}{kT}$ as a function of ionic strength I	
NaCl	pH 4.0	$\frac{\varepsilon}{kT}=0.29543\ \ln\ (I)+3.12532$
	pH 7.0	$\frac{\varepsilon}{kT}=0.232\ \ln\ (I)+3.14678$
$NaNO_3$	pH 4.0	$\frac{\varepsilon}{kT}=0.21362\ \ln\ (\mathrm{I})+3.32364$
	pH 7.0	$\frac{\varepsilon}{kT}=0.14944\ \ln\ (I)+3.29496$
Na_2SO_4	pH 4.0	$\frac{\varepsilon}{kT}=0.155\ [\ln\ (\mathrm{I})]^2+0.25599\ \ln\ (I)+2.96097$
	pH 7.0	$\frac{\varepsilon}{kT}=0.07897\ [\ln\ (I)]^2+0.1601\ \ln\ (I)+2.91088$
NH_4Cl	pH 4.0	$\frac{\varepsilon}{kT}=0.18263\ \ln\ (I)+3.00454$
	pH 7.0	$\frac{\varepsilon}{kT}=0.14031\ \ln\ (I)+3.0025$
$MgCl_2$	pH 4.0	$\frac{\varepsilon}{kT}=-0.13806\ I^2+0.31749\ I+2.79789$
	pH 7.0	$\frac{\varepsilon}{kT}=-0.19402\ I^2+0.3676\ I+2.74608$
NH_4NO_3	pH 4.0	$\frac{\varepsilon}{kT}=-0.07233\ [\ln\ (I)]^2+0.04445\ \ln\ (I)+3.21391$
	pH 7.0	$\frac{\varepsilon}{kT}=-0.13354\ [\ln\ (I)]^2+-0.03813\ \ln\ (I)+3.18738$
$Mg(NO_3)_2$	pH 4.0	$\frac{\varepsilon}{kT}=-0.12094\ I^2+0.38213\ I+2.89999$
	pH 7.0	$\frac{\varepsilon}{kT}=-0.14751\ I^2+0.43055\ I+2.84869$
$(NH_4)_2SO_4$	pH 4.0	$\frac{\varepsilon}{kT}=0.03332\ [\ln\ (I)]^2+0.06235\ \ln\ (I)+2.85676$
	pH 7.0	$\frac{\varepsilon}{kT}=0.22117\ [\ln\ (I)]^2+0.22452\ \ln\ (I)+2.84788$
$MgSO_4$	pH 4.0	$\frac{\varepsilon}{kT}=0.00531\ [\ln\ (I)]^2+0.00561\ \ln\ (I)+2.89747$
	pH 7.0	$\frac{\varepsilon}{kT}=0.00109\ [\ln\ (I)]^2+0.00407\ \ln\ (I)+2.93547$

5. Conclusions

We used a TOA technique to measure CPTs for lysozyme/salt solutions. For the monovalent cations studied, as salt concentration increases, the CPT increases. For divalent cations, as salt concentration rises, a maximum in the CPT is observed and attributed to ion binding to the protein surface and subsequent water structuring. Trends for sulfate salts were dramatically different from those for other salts because sulfate ion is strongly hydrated and excluded from the lysozyme surface. For anions at fixed salt concentration, the CPT decreases with rising anion kosmotropic character. Comparison of CPTs for pH 4.0 and 7.0 revealed two trends. At low ionic strength for a given salt, differences in CPT can be explained in terms of repulsive electrostatic interactions between protein molecules, while at higher ionic strength, differences can be attributed to hydration

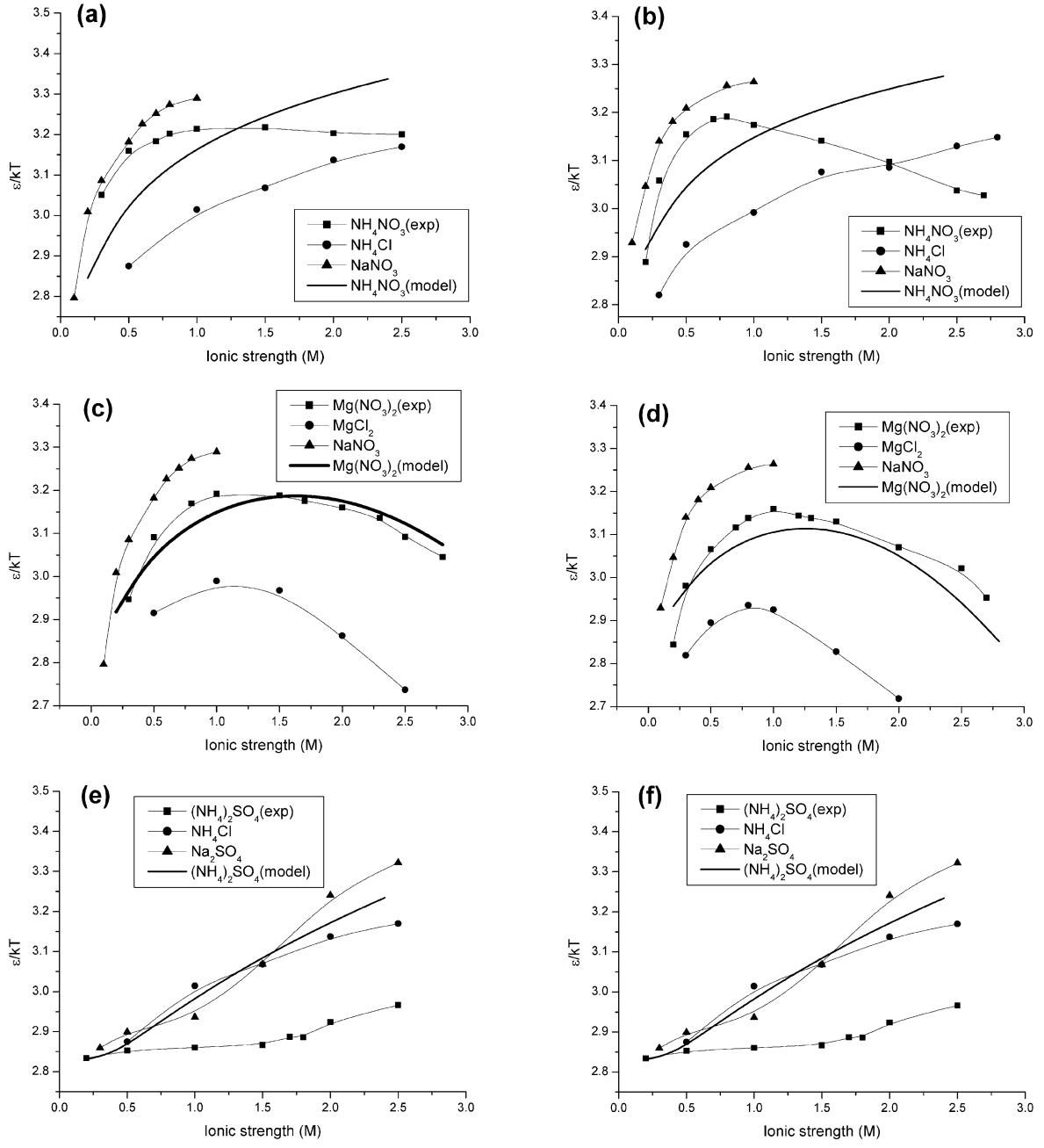

Fig. 10. Plots of the average of $\frac{\varepsilon}{kT}$ for (a) NH_4NO_3 at pH 4.0 (b) NH_4NO_3 at pH 7.0 (c) $Mg(NO_3)_2$ at pH 4.0 (d) $Mg(NO_3)_2$ at pH 7.0 (e) $(NH_4)_2SO_4$ at pH 4.0 (f) $(NH_4)_2SO_4$ at pH 7.0 (g) $MgSO_4$ at pH 4.0 (h) $MgSO_4$ at pH 7.0.

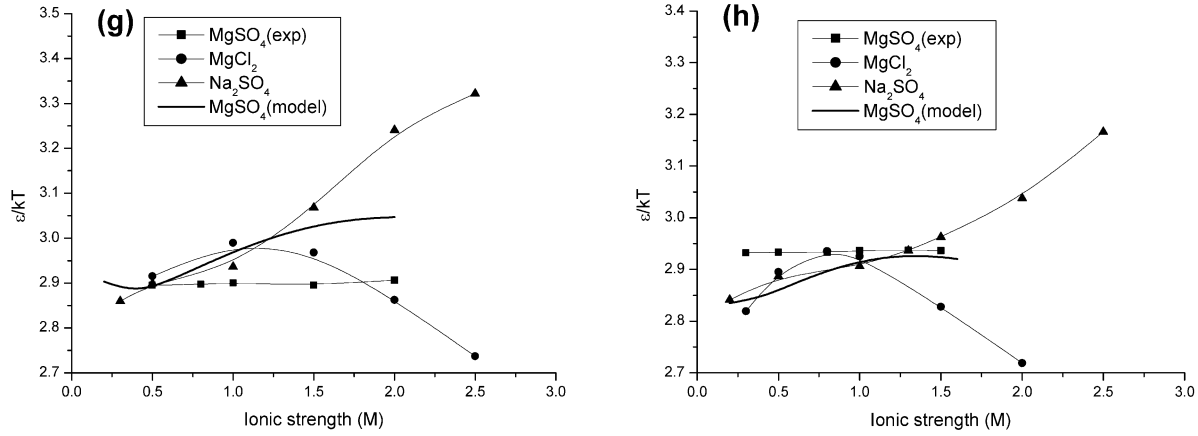

Fig. 10 (Continued).

forces. A model is proposed for the correlation and prediction of the CPT as a function of salt type and salt concentration. NaCl was chosen as a reference salt, and CPT deviations from that of NaCl were attributed to hydration forces. The Random Phase Approximation, in conjunction with a square-well potential, was used to calculate the strength of protein-protein interactions as a function of solution conditions for all salts studied. A more efficient isolation method of protein solutions would be based on predicting the solution conditions, including the cloud-point temperature as a function of protein concentration, salt type, salt concentration and pH, that favor selective precipitation of the target protein.

Acknowledgments

This work was supported by grant No. (R01-2003-10261-0) from the Basic Research Program of the Korea Science and Engineering Foundation. In addition, the authors appreciate great help from Prof. J.M. Prausnitz from UC Berkeley.

References

[1] W.P. Jenck, Binding-energy, specificity and enzymatic catalysis, circe effect, Adv. Enzymol. RAMB 43 (1975) 219–410.

[2] T.S. Burkoth, T.L.S. Benzinger, V. Urban, et al., Structure of the beta-amyloid (10-35) fibril, J. Am. Chem. Soc. 122 (2000) 7883–7889.

[3] B. Drouet, M. Pincon-Raymond, J. Chambaz, T. Pillot, Molecular basis of Alzheimer's disease, Cell Mol. Life Sci. 57 (2000) 705–715.

[4] F. Rothstein, in: R.G. Harrion (Ed.), Differential precipitation of proteins, Dekker, New York, 1994.

[5] M. Muschol, F. Rosenberger, Lack of evidence for prenucleation aggregate formation in lysozyme crystal growth solutions, J. Cryst. Growth 167 (1996) 738–747.

[6] F. Rosenberger, P.G. Vekilov, M. Muschol, B.R. Thomas, Nucleation and crystallization of globular proteins-what we know and what is missing, J. Cryst. Growth 168 (1996) 1–27.

[7] M. Muschol, F. Rosenberger, Liquid–liquid phase separation in supersaturated lysozyme solutions and associated precipitate formation/crystallization, J. Chem. Phys. 106 (6) (1997) 1953–1962.

[8] C.R. Berland, G.M. Thurston, M. Kondo, M.L. Broide, J. Pande, O. Ogun, et al., Solid–Liquid phase boundaries of lens protein solutions, Natl. Acad. Sci. 89 (1992) 1214–1218.

[9] A. Lomakin, N. Asherie, G.B. Benedek, Liquid–solid transition in nuclei of protein crystals, PNAS 100 (18) (2003) 10 254–10 257.

[10] J. Pande, C. Berland, M. Broide, O. Ogun, J. Melhuish, G. Benedek, Suppression of phase separation in solutions of bovine IV-crystallin by polar modification of the sulfur-containing amino acids, Natl. Acad. Sci. 88 (1991) 4916–4920.

[11] M.L. Broide, C.R. Berland, J. Pande, O.O. Ogun, G.B. Benedek, Binary-liquid phase separation of lens proteins solutions, Natl. Acad. Sci. 88 (1991) 5660–5664.

[12] P.A. Darcy, J.M. Wiencek, Identifying nucleation temperatures for lysozyme via differential scanning calorimetry, J. Cryst. Growth 196 (1999) 243–249.
[13] A. Kulkarni, C. Zukoski, Depletion interactions and protein crystallization, J. Cryst. Growth 232 (2001) 156–164.
[14] W.F. Jones, J.M. Wiencek, P.A. Darcy, Improvements in lysozyme crystal quality via temperature-controlled growth at low ionic strength, J. Cryst. Growth 2329 (2001) 221–228.
[15] P.A. Darcy, J.M. Wiencek, Estimating Lysozyme Crystallization Growth Rates and Solubility from Isothermal Microcalorimetry, Acta Cryst. D54 (1998) 1387–1394.
[16] N.M. Dixit, A.M. Kulkarni, C.F. Zukoski, Comparison of experimental estimates and model prediction of protein crystal nucleation rates, Colloids Surf. A 190 (2001) 47–60.
[17] N.M. Dixit, C.F. Zukoski, Crystal nucleation rates for particles experiencing short-range attractions: applications to proteins, J. Colloid Interface Sci. 228 (2000) 359–371.
[18] J. Drenth, K. Kiukstra, C. Haas, J. Leppert, O. Ohlenshlager, Effect of molecular anisotrapy on the nucleation of lysozyme, J. Phys. Chem. B 107 (2003) 4203–4207.
[19] C. Haas, J. Drenth, The protein-water phase diagram and the growth of protein crystals from aqueous solution, J. Phys. Chem. B 102 (1998) 4226–4232.
[20] C. Haas, J. Drenth, The interface between a protein crystal and an aqueous solution and its effect on nucleation and crystal growth, J. Phys. Chem. B 104 (2000) 368–377.
[21] K.W. Derham, J. Goldsbrough, M. Gordon, Pure Appl. Chem. 38 (1974) 97.
[22] M. Gordon, P. Irvine, J.W. Kennedy, J. Polym. Sci. Polym. Symp. 61 (1977) 221.
[23] H. Galina, M. Gordon, P. Irvine, L.A. Kleintjens, Pure Appl. Chem. 54 (1982) 365.
[24] H. Galina, M. Gordon, B.W. Ready, L.A. Kleintjens, in: W.C. Forsman (Ed.), Polymers in Solution, Plenum Press, New York, 1986.
[25] M. Muschol, F. Rosenberger, Interactions in undersaturated and supersaturated lysozyme solutions: Static and dynamic light scattering results, J. Chem. Phys. 103 (24) (1995) 10 424–10 432.
[26] R.B. McClurg, C.F. Zukoski, The electrostatic interaction of rigid, globular proteins with arbitrary charge distributions, J. Colloid Interface Sci. 208 (2) (1998) 529–542.
[27] D.F. Rosenbaum, C.F. Zukoski, Protein interactions and crystallization, J. Cryst. Growth 169 (4) (1996) 752–758.
[28] M. Hloucha, J.F.M. Lodge, A.M. Lenhoff, S.I. Sandler, A Patch-antipatch representation of specific protein interactions, J. Cryst. Growth 232 (2001) 195–203.
[29] S. Ruppert, S.I. Sandler, A.M. Lenhoff, Correlation between the osmotic second virial coefficient and the solubility of proteins, Biotechnol. Prog. 17 (2001) 182–187.
[30] C. Haas, J. Drenth, Understanding protein crystallization on the basis of the phase diagram, J. Cryst. Growth 196 (2–4) (1999) 388–394.
[31] C. Guo, B.E. Campbell, K. Chen, A.M. Lenhoff, O.D. Velev, Casein precipitation equilibria in the presence of calcium ions and phosphates, Colloids Surf. B 29 (2003) 297–307.
[32] Y.J. Yuan, O.D. Velev, K. Chen, B.E. Campbell, E.W. Kaler, A.M. Lenhoff, Effect of pH and Ca^{2+}-induced assocations of soybean proteins, J. Agric. Food Chem. 50 (2002) 4953–4958.
[33] D. Asthagiri, M.R. Schure, A.M. Lenhoff, Calculation of hydration effects in the binding of anionic ligands to basic proteins, J. Phys. Chem. B 104 (2000) 8753–8761.
[34] G.N. Malcolm, J.S. Rowlinson, Trans. Faraday SOC. 53 (1967) 921.
[35] P.R. ten Wolde, D. Frenkel, Enhancement of protein crystal nucleation by critical density fluctuations, Science 277 (1997) 1975–1978.
[36] P.R. ten Wolde, D. Frenkel, Enhanced protein crystallization around the metastable critical point, Theor. Chem. Acc. 101 (1999) 205–208.
[37] D.E. Kuehner, H.W. Blanch, J.M. Prausnitz, Salt-induced protein precipitation: phase equilibria from an equation of state, Fluid Phase Equil. 116 (1996) 140–147.
[38] B.H. Chang, Y.C. Bae, Salting-out in the aqueous single-protein solution: the effect of shape factor, Biophys. Chem. 104 (2) (2003) 523–533.
[39] P. Vimalchand, D. Donohue, Comparison of equation of state for chain molecules, J. Phys. Chem. 93 (1989) 4355–4360.
[40] M.D. Donohue, J.M. Prausnitz, Perturbed hard chain theory for fluid mixtures: Thermodynamic properties for mixtures in natural gas and petroleum technology, AIChE J. 24 (1978) 849–860.
[41] J.N. Isrelachvlili, Intermolecular and surface forces, Academic Press, London, 1985.
[42] G. Waksman, T.S. Krishna, C.H. Williams, J. Kuriyan, Crystal structure of *Escherichia coli* thioredoxin reductase refined at 2 Å resolution, J. Mol. Biol. 236 (1994) 800–816.
[43] Data Bank in National Center for Biotechnology Information, http://www.ncbi.nlm.nih.gov/.
[44] Y.C. Chiew, D.E. Kuehner, H.W. Blanch, J.M. Prausnitz, Molecular thermodynamics of salt-induced protein precipitation, AIChE J. 41 (1995) 2150–2159.
[45] J.J. Grigsby, H.W. Blanch, J.M. Prausnitz, Cloud-point temperatures for lysozyme in electrolyte solutions: effect of salt type, salt concentration and pH, Biophys. Chem. 91 (2001) 231–243.

[46] G.A. Krestov, Thermodynamics of Solvation: Solution and Dissolutions, Ions and Solvents, Structure and Energetics, Horwood, New York, 1991.
[47] O.Y. Samoilov, in: R.A. Horne (Ed.), Water and Aqueous Solutions: Structure, Thermodynamics, and Transport Processes, Wiler-Interscience, New York, 1972, pp. 597–612.
[48] D.E. Kuehner, J. Engmann, F. Fergg, M. Wernick, H.W. Blanch, J.M. Prausnitz, Lysozyme net charge and ion binding in concentrated aqueous electrolyte solutions, J. Phys. Chem. B 103 (1999) 1368–1374.
[49] P. Retailleau, M. Ries-Kautt, A. Ducruix, No salting-in of lysozyme chloride observed at low ionic strength over a large range of pH, Biophys. J. 72 (1997) 2156–2163.
[50] M. Ries-Kautt, A. Ducruix, Inferences drawn from physicochemical studies of crystallogenisis and precrystalline state, Methods Enzymol. 276 (1997) 23–59.
[51] K.D. Collins, Charge density-dependent strength of hydration and biological structure, Biophys. J. 72 (1997) 65–76.
[52] A.C. Cowley, N.L. Fuller, R.P. Rand, V.A. Paarsegian, V.A. Rsegian, Measurement of repulsive forces between charged phospholipid bilayers, Biochemistry 17 (1978) 3163–3168.
[53] R.M. Pashley, DLVO and hydration forces between mica surfaces in Li^+, Na^+, K^+, and Cs^+ electrolytesolutions: a correlation of double-layer and hydration forces with surface cation-exchange properties, J. Colloid Interface Sci. 83 (1981) 531–546.
[54] R.M. Pashley, Hydration forces between mica surfaces in aqueous-electrolyte solutions, J. Colloid Interface Sci. 80 (1981) 153–162.
[55] R.M. Pashley, Hydration forces between mica surfaces in electrolyte-solutions, Adv. Colloid Interface Sci. 16 (1982) 57–62.
[56] R.M. Pashley, J.N. Israelachvili, DLVO and hydration forces between mica surfaces in Mg^{2+}, Ca^{2+}, Sr^{2+}, and Ba^{2+} choride solutions, J. Colloid Interface Sci. 97 (1984) 446–455.
[57] R.M. Pashley, The effects of hydrated cation adsorption on surface forces between mica crystals and its relevance to colloidal systems, Chem. Scr. 25 (1985) 22–27.
[58] J.P. Guilloteau, M.M. Rieskautt, A.F. Ducruix, Variation of lysozyme solubility as a function of temperature in the presence of organic and inorganic salts, J. Cryst. Growth 122 (1992) 223–230.
[59] T. Aarakawa, R. Bhat, S.N. Timasheff, Preferential interactions determine protein solubility in 3-component solution, the $MgCl_2$ system, Biochemistry 29 (1990) 1914–1923.
[60] R.A. Curtis, J.M. Prausnitz, H.W. Blanch, Protein-protein and protein-salt interactions in aqueous protein solutions containing concentrated electrolytes, Biotechnol. Bioeng. 57 (1998) 11–21.
[61] T. Aarakawa, R. Bhat, S.N. Timasheff, Preferential interactions determine protein solubility in 3-component solution, the MgCl system, Biochemistry 29 (1990) 1914–1923.